Complex Viscosity of Block Copolymer Solutions with Models of Microstructural Degradation

G. Scott Hugenberger† and Michael C. Williams*

Chemical Engineering Department, University of California, Berkeley, Berkeley, California 94720. *Received May 12, 1987; Revised Manuscript Received October 15, 1987*

ABSTRACT: Solutions of block copolymers in neutral solvents (those equally good for both block types) form microphase-separated systems like melts when polymer concentration (c) exceeds a certain value (c_s). These structured materials exhibit solidlike properties and are characterized here by measurements of the complex viscosity components η' and η'' as functions of frequency (ω), strain amplitude (γ^0), and $\Delta c \equiv c - c_s$. Tests were made on two styrene–ethylene/butylene–styrene polymers of differing molecular weight (M) but the same styrene content (28%). Extreme sensitivity to γ^0 is found, with properties of most solutions retaining γ^0-dependence down to $\gamma^0 = 0.0005$. The functions $\eta'(\omega,\gamma^0)$ and $\eta''(\omega,\gamma^0)$ are discussed in terms of system microstructure, its alteration due to shear, and its recovery. The parameter Δc is sufficient to characterize M and c dependencies, so that the pattern of $\eta'(\gamma^0)$ and $\eta''(\gamma^0)$ functions can be mapped onto a grid of Δc and ω for both polymers. A new concept of *interface mobility* (movement of block junctions laterally through the domain interphase) is proposed to explain several of these phenomena.

Introduction

The microphase-separated state of liquid block copolymers is of significant engineering importance, inasmuch as processing is usually conducted with the melts or their solutions. This motivates careful study of their rheological properties, which bear all the complexities associated with structured fluids in general and some unique to the block copolymers. Among the rheological features of special interest are the yield stress τ_y (block copolymers may be the only 100% liquid systems with a true τ_y), extreme nonlinearities and thixotropy in steady flow, unexplained stability problems, and sometimes hypersensitivity to amplitude magnitudes in oscillatory testing and other nominally linear-response situations.

The present work, portions of which were reported earlier,[1] is directed toward the use of the complex viscosity ($\eta^* = \eta' - i\eta''$) for characterizing such liquids. Interpretation of data—including dependence on frequency (ω), strain amplitude (γ^0), and polymer concentration (c) in solution—leads to new insight concerning the multiphase microstructure responsible for the observations. It is hoped that some of these observations and insights will be helpful also for understanding other rheologically complex liquids, so the significance of this work should extend beyond the block copolymer area.

A brief review of thermodynamic concepts is useful for placing microstructural concepts in proper perspective. Among several thermodynamic theories for microphase separation, we invoke the Leary model[2,3] which has been further refined recently for bulk polymers[4,5] and was also extended to solutions[6,7] made from good solvents for both blocks—i.e., solvents whose solubility parameter (δ_s) lies between those of the two blocks (δ_A,δ_B) so that solvation of all microphases is considerable. Central to all these cases is the concept of the separation temperature (T_s), with the polymer system nominally homogeneous when $T > T_s$ and in its multiphase condition when $T < T_s$. For good-solvent solutions, $T_s(c)$ is at its maximum at the limit of the bulk polymer and is depressed as solvent concentration increases.

These solvent relationships have been reviewed in some detail;[8] a schematic representation of solvent action is given in Figure 1. There, we emphasize two aspects of $T_s(c)$ that are not generally appreciated. First, from a practical processing standpoint, T_s for the bulk polymer is usually so high that it cannot be reached without substantial material degradation, so bulk polymers must be processed as phase-separated melts with all attendant problems. Our recent investigation of τ_y in a number of such systems[9] was directed toward that situation.

The second point is that solvent can depress T_s to any convenient desired temperature, leading to the situation where a "separation concentration" (c_s) can be defined when isothermal studies are being made; this is also illustrated in Figure 1. Thus, for $c < c_s$ the solution is homogeneous, and for $c > c_s$ the microstructure appears. This explains why the early study by Paul et al.[10] found no rheological peculiarities; although they dealt with "concentrated" solutions, they were facing $c < c_s$ at room temperature. In the present work, we deal exclusively with the c regime near c_s and primarily above it.

Our exploitation of solvent phenomena is very specialized here, as we employ the closest possible approach to the idealized "neutral solvent", defined theoretically[6] as equally attracted to A blocks and B blocks: $|\delta_A - \delta_s|/|\delta_s - \delta_B| = 1$. In such a case, the phase behavior and microstructure (Figure 2) are predicted to mimic those of the bulk polymer, except for obvious scaling of chain densities due to dilution. In this way, one can in principle investigate melt behavior while working at conveniently low temperature where degradation is not a problem.

Previous studies of solution rheology for block copolymers have been relatively rare, and the focus has usually been on cases of "selective solvents"[11–14] where preferential precipitation of one block is the objective for purposes of microstructure control. This also leads to different rheological behavior in certain ways that will be discussed below, and no relationship to melt properties can then be made. To our knowledge, the only previous work reported for neutral-solvent solutions has been by Pico and Williams.[7,15] There, some of the peculiar $\eta^*(c,T)$ behavior was exploited to measure $T_s(c)$, but no effort was made to study the rheology itself.

Experimental Section

Materials. Two KRATON G rubber-type (thermoplastic elastomer) polymers were donated by Shell Development Co., Houston, TX. They had triblock (ABA) molecular structures, the A blocks being polystyrene (S) and the B block being an ethylene/1-butene (EB) random copolymer with 57% ethylene.

† Presently at the State of California Water Quality Board, San Diego, CA.

0024-9297/88/2221-1773$01.50/0

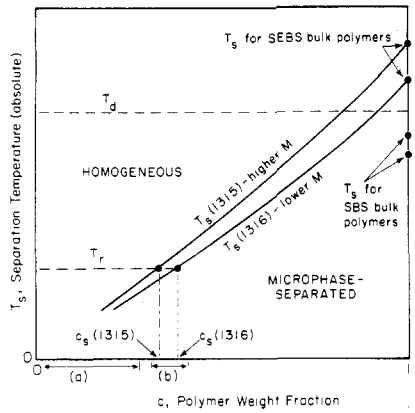

Figure 1. Schematic representation of separation temperature (T_s) dependence on block copolymer concentration (c), when a neutral solvent is used. Room temperature (T_r) and the polymer degradation temperature (T_d) are also shown. Copolymer composition ratio (A/B) and sequence structure (say, ABA) are fixed here. Relative positions of curves for specific types of triblocks are shown (S = A is styrene, B is butadiene, EB is ethylene/1-butene), with the two SEBS polymers representing the ones being used here. Reducing the solubility parameter difference between blocks ($\delta_A - \delta_B$) reduces T_s for both the melt and neutral solutions; it is lower for SBS than for SEBS polymers. Along the abscissa, region (a) designates the range of previous solution studies[10] wherein $c < c_s$ and microphase separation did not occur; region (b) corresponds to the c-range of the present work.

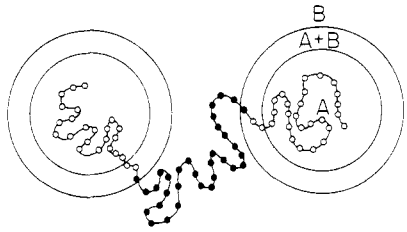

Figure 2. Schematic representation of ABA block copolymer molecule embedded in a phase-separated microstructure consisting of matrix B, core A, and broad interphase of mixed A and B. Cores, here, could be either spheres or cylinders, each being possible for polymers used in this study (28% A). Solvent molecules, if present, are distributed uniformly in neutral solutions.

Both SEBS molecules contained 28% styrene, but they differed in S-block molecular weight: M_S = 10300 for sample TRW7-1315 and 7500 for sample TRW7-1316. Total molecular weights compared in a similar fashion, M_{1315} = 73600 and M_{1316} = 53600, which meant that $T_s(1315) > T_s(1316)$ and $c_s(1315) < c_s(1316)$ according to the theory discussed above;[2,4,6] see Figure 1.

These polymers have sufficiently high M and $\delta_S - \delta_{EB}$ that—according to the Leary theory—T_s apparently cannot be reached without thermal decomposition occurring. Meltlike behavior was achieved by using solutions in dipentene (*p*-mentha-1,8-diene); a technical grade obtained from MCB Chemicals was employed. This solvent has $\delta_{DP} \cong 8.5$ H,[7,8] intermediate between that of the two polymer blocks (δ_S = 9.1 H; $\delta_{EB} \cong 7.9$ H), which makes it very close to a neutral solvent. It was earlier identified[8] as a neutral solvent for SBS copolymers, for which δ_B = 8.1 H. [Symbol H is the Hildebrand unit $(cal/cm^3)^{1/2}$.]

Solutions of the SEBS copolymers—when sufficiently dilute or sufficiently warm—were optically clear and apparently homogeneous, signifying $T > T_s$ at those conditions. Haze formation was evident upon cooling, indicating $T \leq T_s$, and rheological changes occurred simultaneously.

Sample Preparation. A master-batch solution was made of 20–25% by weight polymer. At this concentration, T_s was well below room temperature, and solvation occurred without mechanical agitation; 2 days of standing—with occasional swirling—was sufficient. Solutions of the desired higher concentrations were prepared by adding polymer crumb of known weight to flasks containing master-batch solution, then placing the flasks in a hot oil bath (75–100 °C) and causing them to be steadily rotated (while tilted at an angle) by a gear motor and arm. This procedure, continued for 2–4 days under conditions wherein $T > T_s$, ensured complete dissolution at the higher concentrations.

Specimens for rheological testing were prepared from the hot homogeneous solutions in two very different ways, as described below, and these differences proved to be highly revealing about the phase-separated microstructure that formed upon cooling.

Rheological Apparatus. A Weissenberg Rheogoniometer R17 was employed for η^* measurements. The cone-and-plate geometry had 5-cm platens and a 2.02° cone angle; the torsion bar had a torsion constant of 1801 dyn/cm, a natural frequency of ω_n = 283 rad/s, and a natural time constant (associated with frictional resistance within the bar) of 5.1 s. Readout of input sinusoidal motions of the driven platen (cone) and the output motions of the responding platen (flat plate) were taken from either a two-pen recorder (low ω) or an oscilloscope (high ω). Data analysis followed well-known algorithms,[16,17] including corrections for the movement and inertia of the torque-sensing upper platen and damping by the torsion bar; fluid inertia was negligible.

It was found to be of vital importance, with these SEBS solution samples, to know precisely the angular excursion of the responding upper platen. The *nominal* strain amplitude, γ^0_N, is usually reported in dynamic measurements, but this represents an assumption that the upper platen is immobile. The actual strain amplitude, γ^0, is related to the angular amplitude of input (θ_i) and output (θ_o) motions:

$$\gamma^0 = \frac{1}{\alpha}[\theta_i^2 + \theta_o^2 - 2\theta_i\theta_o \cos\{\tan^{-1}(\theta_o''/\theta_o')\}]^{1/2} \quad (1)$$

where α is cone angle and θ_o'' and θ_o' are the imaginary and real components of the output amplitude. In terms of the measured amplitude ratio of output-to-input waves (AR) and phase angle (ϕ) between the waves

$$\gamma^0 = \gamma^0_N[1 + (AR)^2 - 2(AR)\cos\phi]^{1/2} \quad (2)$$

In our experiments, these corrections were essential; γ^0 was occasionally less than half of γ^0_N, and even when γ^0 depression was less severe, it proved to be important that it be known exactly. This is generally true when amplitude-sensitive materials are being investigated. It may not be widely recognized that, if ω is increased while θ_i is fixed, the resulting θ_o decreases for viscoelastic materials and thus true γ^0 varies (while γ^0_N is constant). When constant-γ^0 tests were desired in the present work (with ω as the independent variable), θ_i was continually adjusted as ω was changed in an effort to maintain the desired strain amplitude in the test specimen.

This analysis is satisfactory when $\theta_0(t)$ signals are sinusoidal (linear response of the given microstructure). Such was the case, or nearly so, in most of the present data, even when the calculated η' and η'' displayed noticeable γ^0-dependence. Under certain rare but important conditions (see Results), the output was nonsinusoidal. In these cases, the same calculational procedure was used (using AR and ϕ taken from the zero-crossing points) even though this lacks rigor. The more rigorous Fourier analysis of wave forms[12,18,19] has previously been employed when nonlinearities were higher order rheological consequences of a constant and uniform microstructure. In the present case, we believe that microstructural changes were involved; this presented difficulties of interpretation with the Fourier method that discouraged its use here. Further analysis will be discussed elsewhere.[20]

All measurements were made at room temperature, in the range of 19–21 °C.

Procedure. Two methods were employed to load samples into the Rheogoniometer, cold-loading and hot-loading. Results were often markedly different.

(a) Cold-Loading. The hot homogeneous solution was poured onto shallow 5-cm diameter aluminum pans and allowed to cool to room temperature in a solvent-saturated atmosphere, covered by aluminum foil which contacted the sample. Thus, no solvent loss occurred and the sample developed no macroscopic concentration gradients in solvent composition. Cooling caused the microphase separation, as the sheet samples became rubbery with sufficient strength to be transferred as solids (gels) to the Rheo lower platen. Lowering the upper platen into position caused a

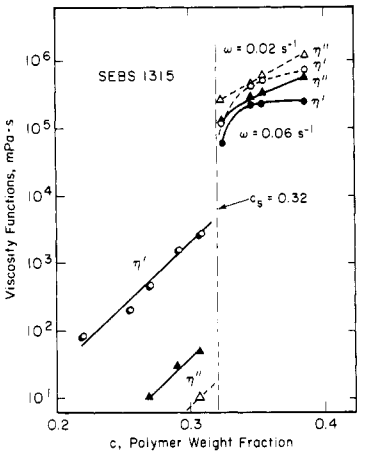

Figure 3. Concentration dependence of η' and η'' when spanning the separation concentration (c_s) at $T \cong 20$ °C. For $c > c_s$, strain amplitude (γ^0) was kept extremely low (0.0005) to preserve microstructure. Solid lines and filled symbols represent testing at $\omega = 0.06$ s^{-1} and dashed lines and open symbols testing at $\omega = 0.02$ s^{-1}. Circles (●, ○) are η'; triangles (▲, △) are η''.

squeezing flow of the sample to occur, thus degrading its microstructure.

(b) Hot-Loading. The hot solution was poured directly onto the lower Rheo platen and the upper platen immediately moved down into position, causing ordinary liquid outflow of the homogeneous sample. As cooling proceeded *in situ*, the microphase eventually formed as $T(t)$ fell below T_s. This microstructure, ideally, would be isotropic, homogeneous, and undegraded. (In practice, a film of structured material may have formed when the hot fluid sample first contacted the cold platen, so homogeneity may not have been perfect.) Solvent loss from the sample during cooling was prevented by using a moat at the platen edge to catch excess material and hold it as a solid barrier which was cut or scraped away immediately before testing.

While extensive data were obtained[21,22] on $\eta^*(\omega)$ at fixed γ^0, special attention was given to measuring $\eta^*(\gamma^0)$ at fixed ω. Such data have not often appeared in the literature, though it is essential for characterizing structured thixotropic materials. Data were taken in a sequence from low ω (or γ^0) to high ω (or γ^0), followed usually by immediate return to low ω (or γ^0) to evaluate the degree of structural change (thixotropy) caused by the initial sequence. Together, these two types of tests help to characterize the $\eta^*(\omega,\gamma^0)$ function and the underlying material microstructure.

Results

Experimental results are presented below in the following sequence: dependence of η' and η'' on concentration (c, weight fraction polymer), on frequency (ω, rad/s), and on amplitude (γ^0, shear strain units). This is followed by a few remarks on nonsinusoidal material response. Interaction and cross-discussion between these topics is necessary and frequent.

Concentration Dependence. We first demonstrate the abruptness of the microphase transition at c_s, by tracking $\eta'(c)$ and $\eta''(c)$ for polymer 1315 in Figure 3. Both functions underwent a discontinuity at about $c_s = 0.32$ (weight fraction polymer), the onset of the transition at about 20 °C.

For $c < c_s$, liquidlike properties prevailed in the sense that $\eta' \gg \eta''$, both functions had low magnitude, and their values were recorded without drift (i.e., no thixotropy was observed because no microstructure existed). Furthermore, those values were independent of γ^0 and thus represented truly linear behavior. The $\eta'(c)$ function was also ω-independent, as demonstrated by identical results at $\omega = 0.06$ and 0.02 s^{-1}, so actually the Newtonian values $\eta_0(c)$ are being shown in Figure 3. As expected, $\eta''(c)$ dropped (open symbol) when ω was reduced, because $\lim_{\omega\to 0} \eta''(\omega) \propto \omega$ for true liquids.

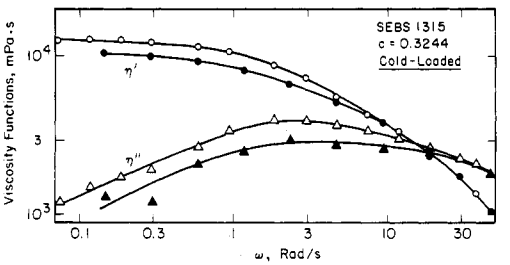

Figure 4. Properties of two cold-loaded samples of polymer 1315 at $c = 0.3244$ (when $c_s \cong 0.32$). Open symbols (○, △) and filled symbols (●, ▲) represent the two samples. Note that ordinary liquidlike behavior is suggested down to the data limit of $\omega = 0.07$ s^{-1}; $0.0007 < \gamma^0 < 0.0032$.

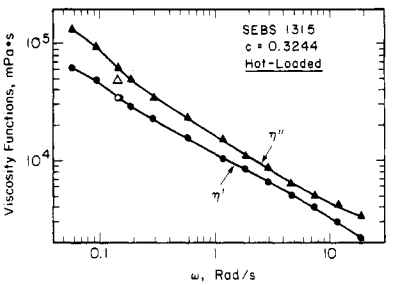

Figure 5. Same solution as in Figure 4, but hot-loaded. Now, solidlike behavior prevails. Filled symbols represent first-run data, taken from low ω to high ω. Open symbols are repeated points, taken immediately after ω_{max} on the first run. (This significance of symbols is used also in all following figures.) $0.0005 < \gamma^0 < 0.0007$.

When $c > c_s$, all evidence indicated solidlike behavior: $\eta'' > \eta'$, high magnitude for both functions, an increase of both when ω was reduced from 0.06 to 0.02 s^{-1}, and a lessened rate of increase with c (markedly so for η'). General experience showed that signals drifted downward with time when c exceeded c_s only slightly—i.e., the microstructure was relatively weak and thixotropic (only stabilized values are reported here)—but at higher c there was usually no drift. However, there proved to be significant γ^0-dependence in both η' and η'' for all structured states, as will be described below. This dependence was most severe when c was only slightly larger than c_s and became less important at higher c, when the structure was stronger. Figure 3 represents conditions at $\gamma^0 = 0.0005$, close to the feasible experimental lower limit of γ^0, but in some cases not representative of a true limiting value for $\eta^*(\gamma^0)$.

In Figure 3 it is obvious that η'' changes much more at c_s than does η' (at low ω and γ^0). This will usually be true, since the liquid → solid transition moves η'' from near zero to a large value while η' changes only from approximately η_0 (already large) to a value larger but still less than the new η''. Thus, η'' is the better indicator of the presence of microstructure. In general, η'' also proves to be more sensitive than η' to the microstructural character (degraded vs virgin, etc.) and thus more helpful for interpreting structural influences on physical properties.

For the 1316 polymer, essentially identical results were obtained. A shift to $c_s \simeq 0.36$ was the major consequence of its molecular weight being lower than that of 1315, as shown in Figure 1 and predicted by the Leary theory modified for the presence of solvent.[6,7]

Frequency Dependence. (a) $c \geq c_s$. At concentrations just above the transition, $\eta^*(\omega)$ is especially sensitive to sample history. This can be seen by comparing data at $c = 0.3244$ (with the 1315 polymer) for the cold-loaded cases (Figure 4) with that for the hot-loaded cases (Figure 5). Figure 4 shows that two cold-loaded samples *seem* to

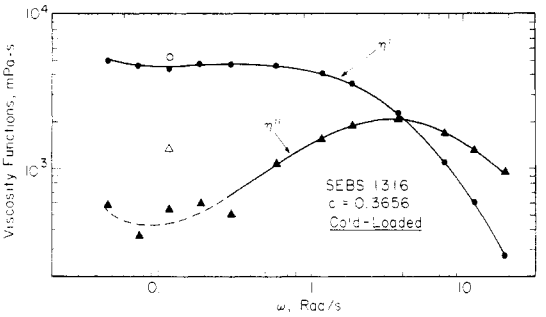

Figure 6. Properties of a cold-loaded sample of polymer 1316 at $c = 0.3656$ (with $c_s \cong 0.36$). Here, $0.0010 < \gamma^0 < 0.0014$.

behave in a liquidlike fashion, with $\eta'(\omega) \rightarrow \eta_0$ and decreasing $\eta''(\omega)$ at low ω. Such data, viewed by themselves, would suggest that $c < c_s$. However, there are two indicators that this is not so. First, the $\eta''(\omega)$ drop at low ω is not quite what is expected of a homogeneous liquid; it is much less steep than ω^{-1}. Second, the η' and η'' curves were not repeatable when two apparently identical samples were tested.

We account for the first observation by presuming that data down to only $\omega = 0.06$ s^{-1} cannot discern that solidlike features will become apparent at lower ω (as will be reinforced below); thus, η' at low ω is not η_0 but merely a plateau from which $\eta'(\omega)$ will increase again at lower ω, and the η'' drop is merely part of a minimum that will likewise increase at lower ω. The second observation reflects the impossibility of reproducing the same degraded microstructure in two cold-loading events. Convergence of data at high ω merely indicates that the high-ω regime is sensitive only to short-range microstructure or molecular influences which are not affected by the breakup of long-range structural elements.

Data for the hot-loaded virgin microstructure (Figure 5) differ dramatically from the cold-loaded case, when $c \geq c_s$. For the entire ω-range $\eta'' > \eta'$, no plateaus or minima are evident, and both functions are markedly larger (for $\omega < 3$ s^{-1}) than their Figure 4 counterparts. Figures 4 and 5 give comparable values only at high ω, again indicating that high frequencies are probing only very short-range features of the microstructure.

Results displayed in Figures 4 and 5 were taken with very low γ^0, in the range 0.0005–0.0007, where γ^0-dependence was weak or nonexistent. The curves could be repeated on the same tested sample, indicating that little or no microstructural alterations occurred at such low γ^0. Figure 5 demonstrates this by displaying repeated points (open symbols, here and hereafter) at $\omega = 0.15$ s^{-1}, taken immediately after the first $\eta^*(\omega)$ run.

The corresponding data for polymer 1316, with $c_s = 0.36$, are given in Figures 6 and 7 (cold- and hot-loaded, respectively). Results are parallel to the preceding ones for the 1315 polymer with $c \geq c_s$. In Figure 6, repeated points at $\omega = 0.12$ s^{-1} show an *apparent* mild recovery, relative to the cold-loaded first run, which was unexpected (but will be explained below). Some additional information on microstructural sensitivity to γ^0 is shown in Figure 7. After $\eta^*(\omega)$ data had been taken on the hot-loaded virgin sample at low γ^0 (<0.0006), the sample was subjected to oscillations at the large amplitude of $\gamma^0 = 0.0075$. Following this, the sample was again tested for $\eta^*(\omega)$ at a low γ^0 (0.0004), producing the reduced values of η^* shown in Figure 7. The conclusion is that exposure to $\gamma^0 = 0.0075$ caused severe microstructural damage, with curve distortions in midrange (i.e., plateau formation and reduced magnitude) that are qualitatively similar to forms seen in Figures 4 and 6 for cold-loaded samples. Now, however, the upturns in η' and

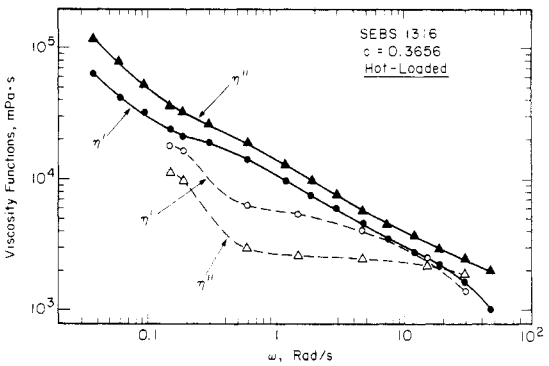

Figure 7. Same solution as in Figure 6, but hot-loaded. In testing the virgin system (filled symbols), $\gamma^0 = 0.0006$ was used. After oscillations at $\gamma^0 = 0.0075$, causing degradation, the second run shown above (open symbols) was obtained at $\gamma^0 = 0.0004$ s^{-1}.

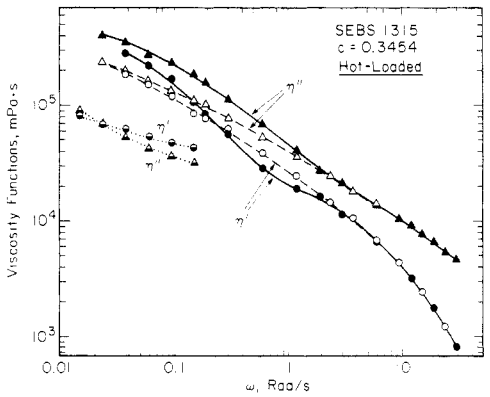

Figure 8. Properties of a hot-loaded sample of polymer 1315 at $c = 0.3454$ (with $c_s \cong 0.32$). Filled symbols represent the virgin system, open symbols the same system altered by oscillations at $\gamma^0 = 0.007$, and half-filled symbols by the properties after a single manual oscillation with $\gamma^0 = 7.1$. Measurements shown here were made with $0.000\,50 < \gamma^0 < 0.000\,58$.

η'' at low ω can be viewed more readily than before, within the accessible range of ω, tending to reinforce our earlier interpretation of the degraded-structure curves from cold-loaded samples.

(b) $c - c_s \cong 0.02$. Increasing the polymer concentration by only a couple percent past c_s caused significant strengthening of the microstructure, as reflected by increased magnitudes of η' and η'' as well as enhanced resistance to degradation.

This is illustrated for hot-loading by the 1315 polymer at $c = 0.3454$, in Figure 8. The virgin structure was characterized ($\gamma^0 < 0.0006$) by η' and η'' values roughly 2–3 times larger than when $c \geq c_s$ (see Figure 5). Then, after oscillations at a large amplitude ($\gamma^0 = 0.007$), the resulting structural degradation was relatively slight, as indicated by retesting at low amplitude (dashed lines and open symbols in Figure 8). Greater degradation was then induced by twisting the platen manually to deliver a sudden strain of $\gamma^0 = 7$. Considerable reduction in η^* occurred, as evidenced by retesting at low amplitude (Figure 8), but not nearly as much as seen in Figure 4 by the cold-loading procedure when $c \cong c_s$.

Results for cold-loading are illustrated by the 1316 polymer at $c = 0.3828$, in Figure 9. The initial cold-loaded structure gave much higher η^* values ($0.0009 < \gamma^0 < 0.0015$) than did the c_s case in Figure 6 and, moreover, did not simulate liquidlike ω-dependence as did the latter. However, the fact that $\eta' > \eta''$ at lower ω for these initial curves in Figure 9 does indicate that some structural damage had been done by the cold-loading procedure. Further degradation was found to occur when the test was

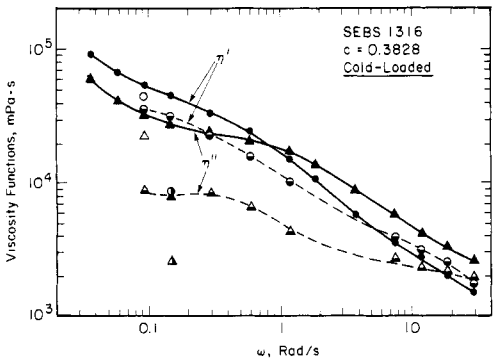

Figure 9. Properties of two cold-loaded samples of polymer 1316 at $c = 0.3828$ (when $c_s \cong 0.36$). Filled symbols represent testing at low strain ($0.0009 < \gamma^0 < 0.0015$), the open symbols being the repeat. Half-filled symbols represent testing at larger strain ($0.0038 < \gamma^0 < 0.0053$), with (◒, ▲) showing tests on a virgin sample and (◑, ▲) being the repeat.

repeated at higher amplitude, $0.0038 < \gamma^0 < 0.0053$, suggesting—by comparison with Figure 8—that the cold-loading damage also predisposed the microstructure to further alterations.

(c) $c - c_s \cong 0.06$. The functions $\eta'(\omega)$ and $\eta''(\omega)$ were similar in shape to those shown for $\Delta c = 0.02$, though of greater magnitude (see Figure 3) and more resistant to degradation. These latter features resulted in part from the lower solvent levels (greater polymer chain densities), but also—for all $\Delta c > 0.02$—from thermodynamic factors to be discussed further below. Basically, the microstructure becomes fully developed when c_s is sufficiently exceeded.

Amplitude (Strain) Dependence. The remarkable sensitivity of the properties of these materials to strain magnitude is already evident in the data presented above. However, a detailed study of the γ^0 functionality provided further insight. This was accomplished by fixing ω at some low value (usually $\omega = 0.15$ s^{-1}) and then varying γ^0 from very low to higher values (but still low, under 0.01). Very few data such as these have appeared in the literature.

(a) Hot-Loading. The major features of $\eta^*(\gamma^0)$ are best presented in the context of an intact and ideal microstructure. Figure 10 shows data for both the highest effective concentration ($c = 0.3861 \cong c_s + 0.066$) and the lowest ($c = 0.3244 \cong c_s + 0.004$), with polymer 1315.

Results are similar for $\eta''(\gamma^0)$ in the two cases—albeit the η'' numerical values differ by nearly an order of magnitude—in the sense that a γ^0-independent linear limit appears to be nearly achieved at low γ^0. Deviations from this as γ^0 increases are only slight until finally a very abrupt drop is registered, and the subsequent decrease is faster than $1/\gamma^0$, a very severe nonlinearity.

Entirely different behavior is found with $\eta'(\gamma^0)$. The weaker microstructure ($c = c_s + 0.004$, Figure 10a) *appears* to yield a Newtonian limit of η_0 and then a rather normal non-Newtonian decrease at higher γ^0. However, the stronger microstructure ($c = c_s + 0.066$, Figure 10b) produces a maximum in $\eta'(\gamma^0)$, with no evidence of a η_0 at low γ^0. Such a phenomenon has apparently not been reported before. It also suggests that the seemingly well-behaved case of the weaker structure may actually be misleading, in that data at lower γ^0 might show a η' maximum there, too.

Another important contrast between these two solutions appeared when, at the end of each run (highest γ^0), a measurement at the lowest γ^0 was repeated. For the weaker microstructure, Figure 10a shows that both η' and η'' failed to recover; η' remained precisely at the same low value it last had (at high γ^0), while η'' managed only a slight

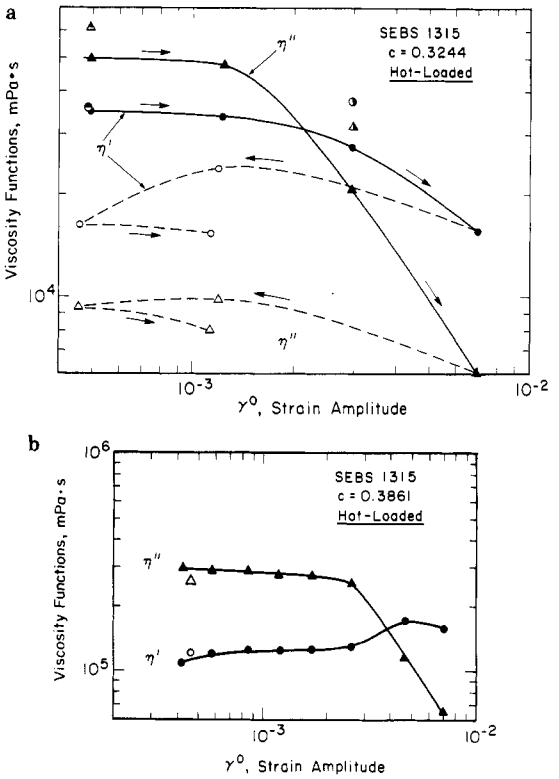

Figure 10. Strain-dependent properties of two hot-loaded solutions of polymer 1315, tested at $\omega = 0.15$ s^{-1}. Filled points represent the original test, from low to high γ^0, and open points the tests which followed the original one. (a) $c = 0.3244$, so $\Delta c = 0.0044$ because $c_s = 0.32$. Arrows show sequence of tests, the repeat sequence defining a continuing degradation pattern. At the beginning, the structure is already degraded from the $\eta^*(\omega)$ run in Figure 5; the first-run values (◒, ▲) are taken from Figure 5. At $\gamma^0 = 0.003$, the values obtained when the new strain magnitude was imposed are designated by (◑, ▲); these correspond to stress waveforms that were visibly nonlinear. These values drifted downward to the points plotted below them. Such drift was seen only with the weakest microstructures and only at certain conditions of γ^0 and ω. (b) $c = 0.3861$, so $\Delta c = 0.0661$. Little structural change resulted from this test, as shown by positions of the repeat points. The maximum in η' was seen also in Figure 10a for the weaker microstructure, on the return run, and may have appeared there in the forward run (●) if more points had been obtained.

recovery from its high-γ^0 value. No changes occurred in such cases during extended periods of waiting, on the order of 10 h.

For the stronger microstructure, however, the initial low-γ^0 values of η' and η'' were almost fully reproduced (Figure 10b). A particularly interesting feature is that the recovering η' was still *higher* than its initial value, indicating a memory for its preceding state at high γ^0 (near the maximum). Thus, the "degraded" microstructure was still giving a higher η' than the original one.

(b) Cold-Loading. These predegraded structures exhibited $\eta^*(\gamma^0)$ behavior very similar to that of the hot-loaded intact structures, so results are taken to be qualitatively general and not artifacts of the loading history.

First, the $c = 0.3861$ solution of 1315 was cold-loaded for comparison with its hot-loaded counterpart in Figure 10. While the magnitudes of both η' and η'' (Figure 11) were reduced by the loading procedure, their γ^0-dependence was not much changed: only the abruptness of the η'' drop and achievement of the η' maximum were mitigated. Lack of appearance of η_0 in the $\eta'(\gamma^0)$ function at low γ^0, as was true also in the hot-loaded case, tends to confirm the generality of it; indeed, this was observed in almost all systems studied. And, once again, this high-c

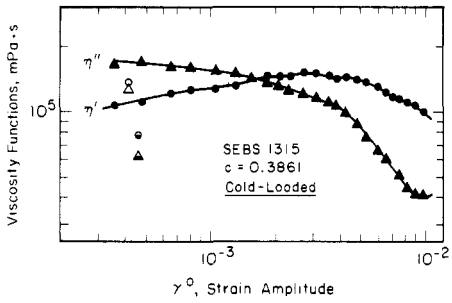

Figure 11. Strain-dependent properties of a cold-loaded solution of polymer 1315, tested at $\omega = 0.15$ s^{-1}. Data-point symbols have same meaning as in Figure 10. The half-filled symbols represent initial readings from a test made after the sample was degraded by a single manually imposed strain oscillation to $\gamma^0 = 7.1$; subsequent cycles of the test showed stress growth, in the direction of previous readings.

solution displayed good recovery properties upon repetition of the lowest γ^0 test after the highest γ^0 (0.01) measurement. However, a more severe degradation—induced by the manual imposition of $\gamma^0 = 7.1$—caused an apparently permanent reduction of property values.

An extensive set of $\eta^*(\gamma^0)$ data on cold-loaded specimens was assembled[22] by using $c = 0.3861$ at $\omega = 0.0237$ and 1.50 s^{-1} (in addition to $\omega = 0.15$ s^{-1}, cited above) for the 1315 polymer, $c = 0.3538$ at $\omega = 0.15$, 1.50, and 15.0 for the 1315 polymer, and $c = 0.3828$ at $\omega = 0.15$, 1.50, and 15.0 for the 1316 polymer. The "effective" concentrations, $\Delta c \equiv c - c_s$, were approximately 6.6, 3.4, and 2.3 $\times 10^{-2}$ in these cases, respectively.

Variation of ω led to significant changes in the $\eta'(\gamma^0)$ and $\eta''(\gamma^0)$ patterns for each solution. The direction of these pattern changes was the same, however, for all three systems. A matrix, designed to illustrate the trends (with Δc and ω) as well as to display all nine data sets, is presented in Figure 12. It is clear that the *shapes* of $\eta'(\gamma^0)$ and $\eta''(\gamma^0)$, together with their *relative positions*, evolve with ω and with Δc in a consistent fashion. A Δc–log ω symmetry is suggested in the layout. While a few minor defects appear in the pattern—possibly due to problems in reproducing the cold-loaded microstructure—the major

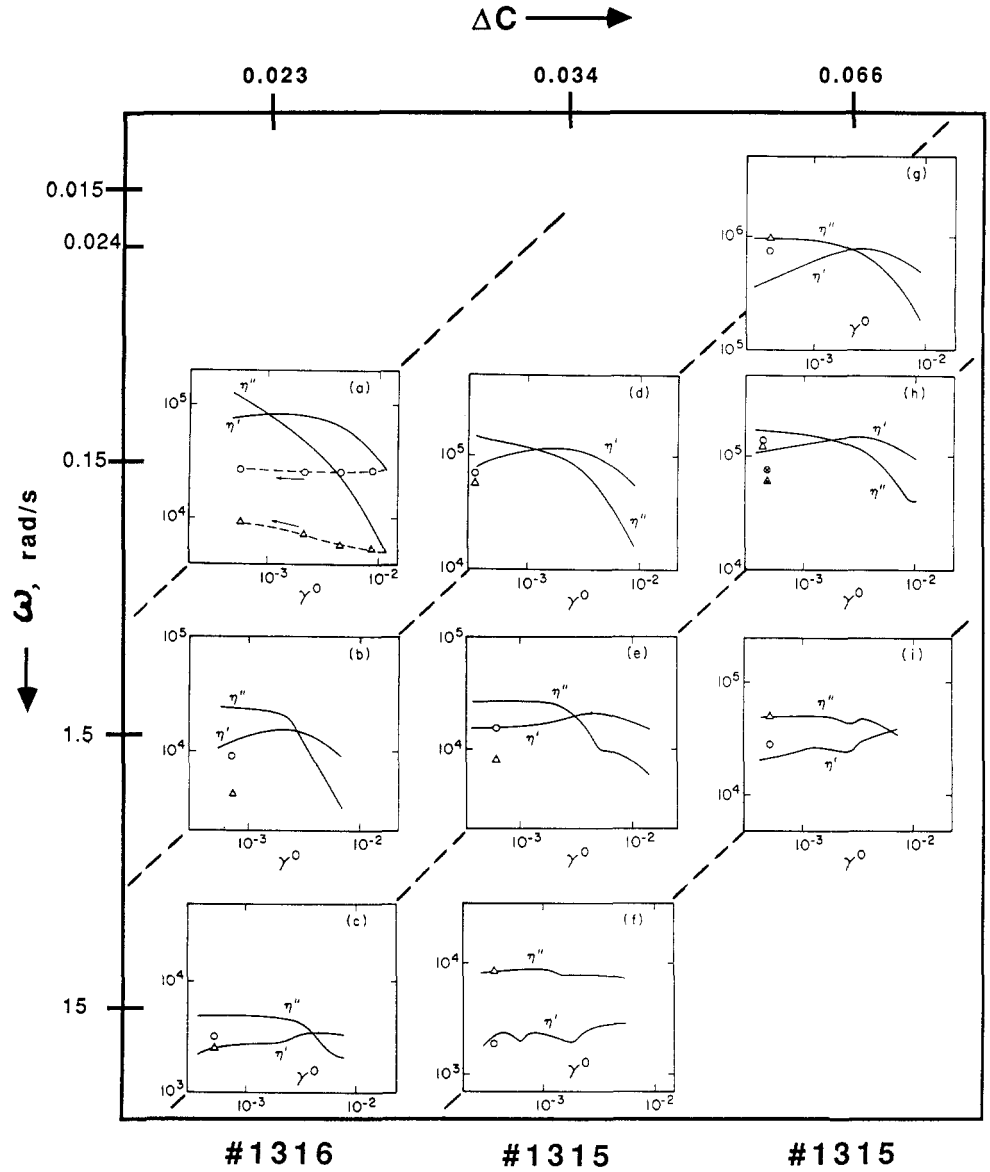

Figure 12. Composite of strain-dependent properties of cold-loaded samples of polymers 1315 and 1316. Values of ω and $\Delta c = c - c_s$ for each pair of $\eta'(\gamma^0)$ and $\eta''(\gamma^0)$ curves are read from the composite axes. Smooth curves—data points available elsewhere[21,22]—represent initial testing of the as-loaded samples and open symbols the repeated tests upon return to low γ^0. (Note Figure 12h is the same as Figure 11.) Diagonal dashed lines connect data sets having similar patterns, unifying results for systems with different Δc and M at different ω.

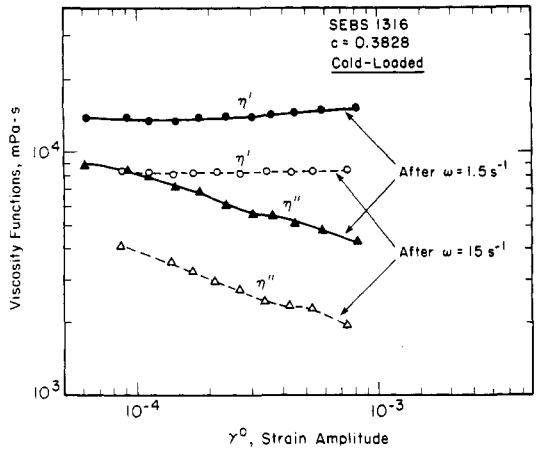

Figure 13. Influence of ω on the levels of microstructural alteration caused by $\eta^*(\gamma^0)$ tests to $\gamma^0 = 0.0075$. Two different samples of cold-loaded 1316 solution ($c = 0.3828$) were tested, one at $\omega = 1.5$ s^{-1} (filled symbols) and one at $\omega = 15.0$ s^{-1} (open symbols). Then, data above were obtained at $\omega = 0.15$ s^{-1}.

features seem helpful in correlating the variables.

The degree of microstructural recovery after imposition of the largest γ^0 is also shown for each system in Figure 12, as reflected by repeated tests of η' and η'' at the lowest γ^0 values.

For the $\Delta c = 0.023$ and 0.034 systems, the recovery of η' was usually nil; the repeated low-γ^0 values of η' were identical with the high-γ^0 values. When $\eta'(\gamma^0)$ had dropped, then the repeated low-γ^0 η' remained low (Figures 12, parts a, b, and d); when $\eta'(\gamma^0)$ had increased, the repeated low-γ^0 η' remained high (Figure 12c); and when $\eta'(\gamma^0)$ happened to terminate at a value identical to the original one—after going through a maximum (Figure 12e)—then the original (final) value was reproduced. Only for the highest ω testing (15.0 s^{-1}) with the stronger microstructure ($\Delta c = 0.034$) was a true η' recovery seen (Figure 12f).

This latter observation suggests that the combination of stronger thermodynamic driving force (Δc) together with an energy source (high-ω oscillations) can achieve recovery in finite time, with the mechanical energy input being critical for overcoming energy barriers to the recovery. For the $\Delta c = 0.066$ system, no run was made at $\omega = 15.0$ s^{-1}, so this speculation about mechanical-energy-driven recovery (suggested by data at $\Delta c = 0.034$) cannot be tested in the same way with another high-Δc solution. However, similar trends are shown at lower ω: at $\omega = 1.5$ s^{-1}, this solution exhibited partial η' recovery (Figure 12i) as gauged by the "return ratio" $\eta'_2/\eta'_1 \cong 1.3$ (at $\gamma^0 = 5 \times 10^{-4}$). Less recovery was seen at the two lower frequencies (Figure 12, parts g and h), with $\eta'_2/\eta'_1 \cong 1.8$ at $\omega = 0.0237$ s^{-1} being poorest and the $\omega = 0.15$ s^{-1} case intermediate.

These two latter cases were unique in another way, being the only ones wherein the repeated low-γ^0 test of η' appeared to climb back from the "degraded" high-γ^0 value to a point substantially *higher* than the initial low-γ^0 measurement. For both, the $\eta'(\gamma^0)$ curves had maxima and the repeated low-γ^0 tests produced η' values approximating those maximum values rather than the "degraded" values at high γ^0. While quite surprising, this phenomenon is probably a manifestation of the *degraded* microstructure possessing a $\eta'(\gamma^0)$ curve—not measured here—with a maximum shifted to lower γ^0 (say, near the initial γ^0). Such peculiarities are not unlikely to accompany the thixotropic nonlinear rheology of structured materials.

Recovery of η'' after the $\eta''(\gamma^0)$ test was always greater than η', and it was never zero. For the weakest microstructure, $\Delta c = 0.023$, η'' recovery was also the smallest (Figure 12, parts a–c) and nowhere close to original values.

Figure 14. Output stress response to a sinusoidal input strain, for fixed strain amplitude $\gamma^0 = 8.10 \times 10^{-4}$: (a) $\omega = 0.0376$ s^{-1}; (b) $\omega = 0.0596$ s^{-1}; (c) $\omega = 0.0945$ s^{-1}; (d) $\omega = 0.150$ s^{-1}. (Changes in chart speed are responsible for apparent deviations in frequencies displayed here.) Sample is a hot-loaded solution of polymer 1316 at $c = 0.3656$ (so $\Delta c \cong 0.005$).

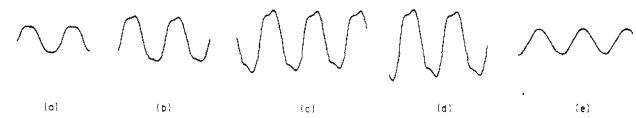

Figure 15. Output stress response to a sinusoidal input strain, for fixed frequency $\omega = 0.15$ s^{-1}: (a) $\gamma^0 = 0.000\,89$; (b) $\gamma^0 = 0.001\,16$; (c) $\gamma^0 = 0.001\,51$; (d) $\gamma^0 = 0.001\,89$. Parts a–d represent the same sample as in Figure 14, a sequence which followed that in Figure 14. Then, a major change in microstructure occurred with a manually imposed single cycle of oscillation to $\gamma^0 = 7.1$, after which the response in (e) was seen.

When $\Delta c = 0.034$, results were again mixed—poor recovery at the lower ω but essentially perfect at $\omega = 15.0$ s^{-1} (as was true also for η'), as shown in Figure 12f. With $\Delta c = 0.066$, η'' always recovered well and perfectly at $\omega = 1.50$ s^{-1} (Figure 12i).

Despite this commentary being oriented toward the role of γ^0 in altering microstructure, the role of ω also needs to be appreciated because its magnitude also affects degradation. This is demonstrated in Figure 13, for two initially identical solutions that had just been tested for $\eta^*(\gamma^0)$ at different frequencies ($\omega = 1.50$, 15.0 s^{-1}) up to $\gamma^0 \cong 0.007$. Following that, they were both tested again at very low frequency ($\omega = 0.15$ s^{-1}) and low γ^0 (only to $\gamma^0 = 0.0008$) to preserve what microstructure they had at the conclusion of the previous measurements. As Figure 13 shows, dramatically different results were obtained; both $\eta'(\gamma^0)$ and $\eta''(\gamma^0)$ were affected in the same way, with values only half (after the $\omega = 15.0$ s^{-1} test) of those produced after the $\omega = 1.5$ s^{-1} test.

Nonsinusoidal Responses. Reproducible nonlinearities, of a sort not reported heretofore, were seen in the output signals when three conditions were met: Δc very small (i.e., $c \cong c_s$), ω small, and γ^0 small. In all cases, the input motion was perfectly sinusoidal. Typical results are displayed in Figures 14 and 15 for a hot-loaded sample of polymer 1316 at $\Delta c \cong 0.006$.

In Figure 14 the dependence on ω is seen, with the magnitude of ω small ($0.0376 < \omega < 0.150$ s^{-1}) and γ^0 also small (8.1×10^{-4}). The nonlinearity—manifested as elbow-shaped extrema in the wave—could not be eliminated even at the mildest measurable conditions. At $\omega = 0.0376$ s^{-1}, this peak was symmetrical, but as ω increased, an asymmetry became evident; also, the peak became less pronounced as the shoulder rose from the left side of the wave. When $\omega = 0.15$ s^{-1}, this produced a squared-off impression with some asymmetry. At still higher ω (> 1 s^{-1}), stress outputs again became sinusoidal.

The effect of γ^0 is seen in Figure 15 with $\omega = 0.15$ s^{-1} and γ^0 increased from 8.90×10^{-4} to 18.9×10^{-4}. The initial condition (Figure 15a) represents only a slight change from Figures 14d (γ^0 increased by 0.8×10^{-4}), but the waveform is seen to be even more flattened. Increasing γ^0 by another 2.7×10^{-4} (Figure 15b) produced a new phenomenon, another shoulder-and-peak rising at the crest and the shoulder developing into a minipeak at higher γ^0 (Figure 15d).

These evolving waveforms were not tracked to higher γ^0, but we can speculate that eventually—at very high

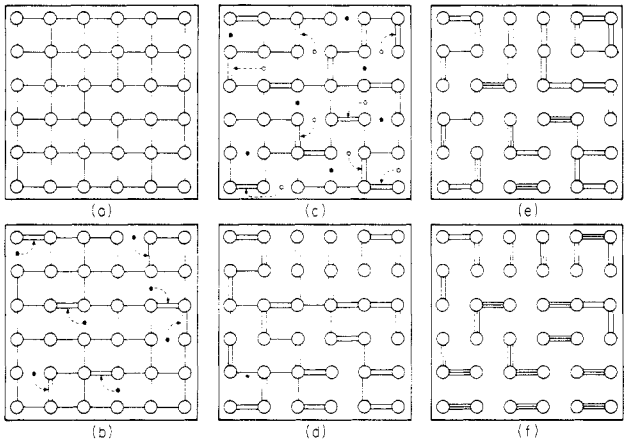

Figure 16. Schematic representation of ABA microstructure topology, for various levels of structural perfection. (a) Virgin structure, equal numbers of B-block chains connect each A core with each of its neighboring cores. (b) Initial stage of degradation, with seven interconnections between nearest-neighbor cores being eliminated. (This would also alter some core volumes, though not shown here.) Filled circles (●) represent vacated positions of B connectors, the dashed arrows showing how the new connections are made. The resulting structure is not only weaker as a solid—though this is not obvious from the sketch, since some intercore connections have doubled their number of B-connectors—but also the structure begins to show more liquidlike character. (c) Further degradation, with a total of 15 interconnections between cores being lost. Open circles (○) show the newly vacated positions of B-connectors, the filled circles from (b) being retained too. (d) Major degradation and rearrangement. Here, some "tie" molecules are allowed to be displaced in two steps—i.e., two A-block withdrawals—so they now appear as connectors between cores different than either of their originating ones. Also, some previously disconnected cores have been reconnected. The net result if that 25 intercore connections are now lost, but the three-dimensional network is marginally preserved. Major liquidlike behavior is manifested, at least down to only moderately low ω. (e) Loss of three-dimensional connectivity, with conversion to a liquid that consists of large suspended chunks of locally connected cores. (f) Further degradation, as chunks become smaller and the cores more strongly bound to each other.

γ^0—the microstructure would be substantially degraded and the waveforms would become sinusoidal again. This contention is supported by results following a manually imposed large strain ($\gamma^0 = 7.1$); Figure 15e shows that the same test conditions as in Figure 15d produced now an output much closer to sinusoidal.

Discussion

The mosaic of data presented here represents a severe challenge to theoretical modeling, even for such a "simple" flow as small-amplitude sinusoidal shear. The origin of anomalies lies in the microstructure, and, most importantly, how it changes in response to the shear. In different types of tests, these same materials would manifest a strongly non-Newtonian viscosity with no apparent η_0 limit, yield stress, and thixotropy. Those phenomena need to be modeled, too, and we hope that the clarification of sinusoidal dynamic response will assist with this or at least provide some guidelines for channeling theoretical ventures.

No mathematical models will be constructed here, although such work[22] will be presented separately.[20] Our present objective is merely to provide a conceptual framework for future discussions and to use this to propose explanations for some of the phenomena shown above.

Microstructure. Figure 2 for ABA polymers is extended to a larger spatial domain in Figure 16, in a purely schematic fashion. An idealized (hot-loaded?) microstructure is represented in Figure 16a as having equal numbers of B connectors between the discrete cores of A. The first stage of structural alteration (Figure 16b) due to small deformation causes repositioning of the chains, but in such a way as to return all A blocks to cores; this will be thermodynamically favored. The precise configuration of these repositioned chains will depend on the nature and magnitude and duration of the deformation, but for convenience Figure 16b is drawn without such complications as loops that put two A blocks from the same molecule into the same core—i.e., the number of B links between cores is a constant throughout Figure 16.

It should be noted that, in discussing small-amplitude shear, we can ignore the possibility of "chunk flow", in which large regions of the material tear loose and are displaced while their internal microstructure is preserved. Such phenomena will probably have to be described when steady flow and other large-deformation phenomena (including cold-loading, possibly) are modeled. Figure 16, however, can realistically retain the concept that the lattice of A cores remains intact under strains no greater than 0.1%, as was the case in the present experiments.

Further deformation (unspecified at present) leads to further structural alterations, represented in Figure 16, parts c–f. An important stage is the change in Figure 16 from part d to part e, with loss of three-dimensional network character and full interconnectedness of the cores. (It seems possible that cold-loading accomplishes something like this.) Note that *microstructure still exists*, the cores remain in place and of similar size (as drawn) but the material has changed from a solid to a liquid. A rheological transition thus occurs, though a measurement of "structure" via local density variations (e.g., by X-ray scattering) would sense no change. However, true microstructure—as measured by topological features as well as others—would certainly have changed, even though $T < T_s$. The new microstructure would therefore not be at equilibrium but could be extremely stable because of kinetic factors hindering its return to equilibrium.

Further structural degradation (Figure 16f) would lead ultimately to a limiting case; this might be a "dimer" limit, though we do not discount a possible "monomer" limit of nonconnected cores. Beyond this point, flow and deformation would be very easy and structure would be difficult to detect rheologically. Conceivably, a limit without structure—i.e., with chemical homogeneity—might be reached at high shear rates $\dot{\gamma}$, for mechanical reasons or thermodynamic reasons (strain-induced depression of T_s, so that $T_s(\dot{\gamma})$ becomes less than ambient).

Degradation Effects on $\eta^*(\omega)$. Microstructural degradation was shown for $\eta'(\omega)$ and $\eta''(\omega)$ in many ways. The trauma of cold-loading was evident in comparing Figure 4 to Figure 5 and also Figure 6 to Figure 7; sinusoidal oscillation to even moderate amplitude (Figures 8 and 9) also revealed structural alterations. The entire set of data[21,22] suggests that the pattern of $\eta^*(\omega)$ change with degrading microstructure should look like Figure 17. The hot-loaded ideal system, corresponding to the microstructure in Figure 16a, would produce the curves labeled (a) in Figure 17 (solidlike, maximum "strength", with τ_y). When topological degradation is complete (e.g., Figure 16f), the curves labeled f in Figure 17 should be seen. Note that the rheology of each state is linear, and results change only because of structural state alteration.

It was generally found that degraded microstructures, when retested for $\eta^*(\omega)$ after an initial measurement that caused the degradation, gave a response at high ω identical to or close to the initial one (even through η^* was appreciably altered at low ω). This is illustrated in Figures 7–9.

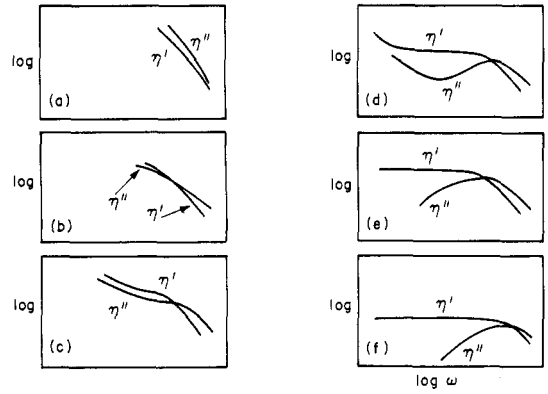

Figure 17. Evolution of $\eta^*(\omega)$, as measured at very low γ^0, due to increasing degradation of the initial ABA microstructure. Thus, the measured pattern can be interpreted in terms of structural topology. For example, the initial $\eta^*(\omega)$ behavior above corresponds to the microstructure in Figure 16a, and the final two $\eta^*(\omega)$ displays represent the structures in parts e and f of Figure 16.

This arises because of the coupling between a specific size scale of the microstructure and a specific ω. Thus, at low ω, large-scale features of the microstructure (three-dimensional connectivity over large regions) are responding, and consequently the weakening of long-range structure is detected at low ω. These features of degradation may not be accompanied by changes at the short-range microstructural level, and in such a case the high-ω measurements would not reflect any differences in repeated tests.

Such arguments make clear that high-ω data are not definitive for assessing structural degradation; moreover, moderate-ω data may be misleading in producing some liquidlike manifestations (e.g., Figure 4) in a degraded microstructure but missing the low-ω evidence of three-dimensional interconnectedness still being retained. The implication is that a very wide spectrum of ω is needed to characterize accurately the microstructure of these materials and to avoid misleading conclusions from dynamic rheological data.

Effective Concentration, Δc. The transition onset, c_s, is very abrupt, but structural development appears to continue to slightly higher concentrations. Solidlike cohesiveness seems to correlate with $\Delta c \equiv c - c_s$, presumably for thermodynamic reasons, and Δc also absorbs M-dependence through $c_s(M)$. For example, the marked enhancement in η' which occurs when c increases merely from $\Delta c = 0.004$ to $\Delta c = 0.023$ (the first two η' points with $c > c_s$ in Figure 3) cannot be explained by the very small increase in polymer chain density.

We propose that the transition breadth in c corresponds to the breadth of the molecular weight distribution (MWD). For a monodisperse MWD, the entire microstructure should form at c_s according to theory.[6] However, even a small polydispersity causes a c-range for structure development. Once the thermodynamic transition has been fully accomplished, the resulting topological structure should grow in strength only slowly with further increase in c (as is indeed shown in Figure 3). Thus, the c-pattern for $\eta^*(\gamma^0;\omega,\Delta c)$ in Figure 12 probably represents $\eta^*(\gamma^0;\omega)$ initially evolving with structure development (near the completion of the thermodynamic transition) and then continuing due to a linear increase of interdomain connecting chains.

The existence of such a c_s-range for isothermal neutral solutions of ABA polymers is analogous to melts having a T_s-range when the MWD is not monodisperse. For melts, the T_s-range (arising from a MWD) was proposed earlier[9] in connection with the continued growth of τ_y as cooling occurred for a nominally monodisperse styrene–butadiene–styrene polymer. In that case, τ_y increased throughout at least a 40-degree range below T_s (150 °C), giving $\Delta T/T_s \cong 0.095$. This is very similar to the case here; since the full range of the transition for polymer 1315 is about $\Delta c \cong 0.03$, one obtains $\Delta c/c_s \cong 0.03/0.32 \cong 0.09$ at the least. The similarity of these phenomena demonstrates again the utility of working with neutral solutions to investigate or predict melt behavior.

Significance of $\eta^*(\gamma^0)$. Incorporating this rarely measured behavior in a theoretical model will be difficult, as it seems to reflect very sensitively the details of microstructural perfection. For the present systems, it was almost impossible to achieve sufficiently low γ^0 for the data to become independent of this parameter in a truly limiting sense. Over certain small ranges of γ^0, and typically at small γ^0, η' and η'' became simultaneously approximately constant; however, this did not prevail at the lowest γ^0, so a limiting condition was not really reached. The general pattern (Figures 10–12) was that an initial increase of γ^0 from the lowest possible value caused η'' to decrease steadily (albeit only slightly when Δc and ω were large) and η' to increase. For some degraded structures (Figure 13), η' appeared to be γ^0-independent at low γ^0, but these systems clearly lacked sensitivity because their large-scale network had been lost; even in these cases, however, η'' was still γ^0-dependent. Generally, small-Δc systems were most sensitive to γ^0 and large-Δc systems least so.

Particularly intriguing was the maximum in $\eta'(\gamma^0)$, which has apparently not been reported before. While rather puzzling, it probably reflects the fact that an increasing γ^0 is causing structural degradation (see Figure 16) which first causes a shift toward more liquidlike behavior (increasing η' and decreasing η'') before the microstructure itself weakens so much that both properties deteriorate at higher γ^0. This explanation is also consistent with the observation (e.g., Figure 13) that the $\eta'(\gamma^0)$ maximum is often eliminated after the first $\eta^*(\gamma^0)$ run.

Structural Recovery. Following a $\eta^*(\gamma^0)$ test, η' and η'' usually remained nearly at their final high-γ^0 values for extended periods of time, as assessed by repeating a single-point low-γ^0 measurement. This single low-γ^0 point is here taken to characterize the *recovered* form of the degraded microstructure, but it should be recognized that this is only a very incomplete characterization. It is certainly possible that two different microstructures could produce similar η^* values at a single γ^0, and this could be erroneously interpreted here as indicating that a degraded system had fully recovered its original microstructure. However, in the absence of the full $\eta^*(\gamma^0)$ function for the degraded system, we will adopt the *convention* that microstructural recovery is gauged by closeness of return of η' and η'' to their original values in a single very low-γ^0 measurement. Thus, the result of this test was to infer that microstructure *usually* did not recover appreciably from the degraded state achieved at highest γ^0 in the preceding $\eta^*(\gamma^0)$ run. Under some conditions, it appeared that partial recovery had taken place, as the repeated low-γ^0 test came close to (but remained below) the original η^* values. This behavior was displayed in Figure 12 and discussed earlier to some extent.

The position we take is that, to a first approximation, the microstructure existing after tests at the largest γ^0 ($= \gamma^0_{max}$) will be preserved in further testing as long as $\gamma^0 \leq \gamma^0_{max}$. However, this does *not* mean the degraded microstructure will—when tested as before—produce η^* data independent of γ^0. All we can expect is that the new $\eta'(\gamma^0)$

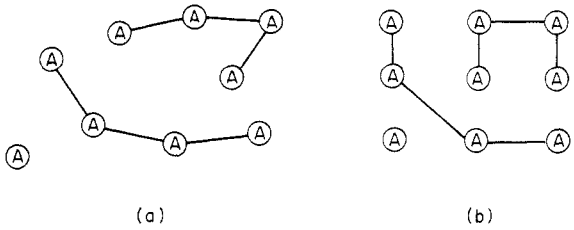

Figure 18. Domain configurations can differ without altering the topology defined by interdomain chains connecting them. (a) Disordered configuration, such as might be caused by η^* measurements or other macroscopic deformations. (b) Ordered configuration, obtained from (a) by a diffusional process abetted by tensions in interdomain chains. (A square lattice is used here only to be consistent with Figure 16; it is likely that an hexagonal lattice would be the actual equilibrium state.)

and $\eta''(\gamma^0)$ curves will differ from the earlier ones. Also, these will be *isostructure* curves, with the topology not changing during the repeated test. A similar proposal was made by Jones and Brodkey[23] in the context of evaluating thixotropic suspensions.

Most commonly, points along the isostructure $\eta^*(\gamma^0)$ curves will be below the preceding ones, and the γ^0-dependence will also be far less sensitive than before. However, some γ^0-dependence is often possible, and indeed this was our explanation for the apparent anomaly (Figures 10b, 12g, 12h/11, and 12i) that η' in the second low-γ^0 measurement was higher than the initial one.

To a second-order approximation, the structural degradation and recovery appear to depend also on ω (Figure 12) and not just on γ^0. Some of this ω-dependence is only a manifestation of the fact that the structural size scales being probed depend on ω, as argued above, but some of it reflects real variations in degradation of microstructure (as Figure 13 proves). The degradation mechanisms can indeed differ with ω—e.g., during a shear cycle at low ω the local interconnected units have sufficient time for local stress to be relieved by intraphase Brownian diffusion of chains and by lateral movements of block junctions within the interphase (see following discussion of "interface mobility"). Thus, at low ω, local damage to domain cores can be avoided or repaired before the next cycle, while at high ω this process has less time to be enacted. Another factor, unrelated to time scales, is the applied stress itself; at higher ω (with fixed γ^0_{max}) the stress is also higher, which is expected to cause more degradation. Both mechanisms are probably involved here. Thus, microstructures achieved at γ^0_{max} will be truly different for different-ω tests, and the repeated low-γ^0 points will reflect this.

For long-term static recovery, some very gradual changes seem to occur in the repeated low-γ^0 and low-ω data. This does not mean that the original three-dimensional topology is being reconstituted but only that the "reduced" microstructure is evolving in a fashion which does not involve restoration of the original topology. For example, in Figure 16e the reduced microstructure contains "triplets" (three domains connected linearly) which may be in relatively unfavorable configurations when first formed—e.g., right-angle sequences—but which relax into more favorable states over a long period. This would not mean that the virgin microstructure of Figure 16a would ever be restored. One mechanism for this sort of recovery is the slow diffusion of the cores and other interconnected units to relieve local stresses by improving the core lattice arrangement; this process is diagrammed in Figure 18, though the drawing is exaggerated (large γ^0) for illustrative purposes. Another recovery mechanism, which can also be coupled with the previous one, is the rearrangement of the configurations of individual chains that had assumed high-

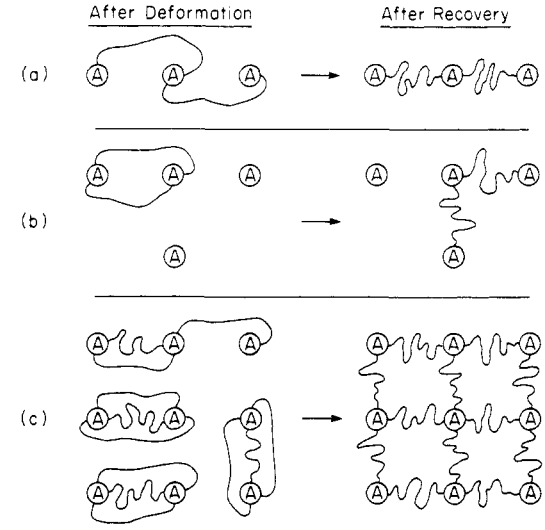

Figure 19. Metastable (thermodynamically unfavored) topologies could arise as a consequence of sample deformation. (a) Two-chain example with no pullout of A blocks from cores. Chains initially in an unfavored high-strain condition would prefer to rearrange to low-strain positions. This is easy and rapid if interface mobility is high. (b) Two-chain example where each chain rearranges with one A-block pullout. If the A blocks emerge from their original core before interface mobility permits other (more favorable) rearrangement, then they will seek different cores that offer a connection with less strain. (c) Degraded system, with liquidlike character, has many high-strain connections between neighboring cores. Systems with high interface mobility can relieve strain without topological change (not shown; see (a)). For others, a high thermodynamic incentive remains to restore the interconnections of cores and thus relieve a multitude of local strains (displayed above). It is clear that additional bulk deformation could assist this process; see Figure 20.

energy states during the degradation process.

Central to the latter mechanism is the concept of *interface mobility* of the chains penetrating through the interphase, from the A core to the B matrix. It is clear that some of the molecular linkage between cores in the degraded microstructure involve enhanced molecular tension and consequent nonequilibrium states. If the interphases are sufficiently fluid, A–B chain junctions can move laterally in the domain surface without disrupting the topology at all; this process is illustrated in Figure 19a. Thus, for at least these two reasons, some measure of property recovery will be seen as the isostructure state approaches its own equilibrium.

While topological recovery should not occur (in finite time) and the γ^0_{max}-fixed microstructure should be preserved, there remain thermodynamic forces favoring such a recovery; see Figure 19, parts b and c. Any agency capable of providing the energy required to surmount the kinetic barriers to such a process will cause the recovery to occur. It would be necessary to transfer energies comparable to the thermodynamic ones[24] retarding the pullout of A blocks from their cores.

This is the context by which we explain some dramatic recoveries that were seen, upon occasion, when mechanical energy was introduced by retesting degraded systems. The clearest example of this is shown in Figure 20, for a cold-loaded sample of 1315 at $c = 0.3272$ ($\Delta c \cong 0.007$). The initial response was that of a liquid, but the wave amplitude grew and the phase angle decreased with time under constant-ω and constant-γ^0 conditions. This led, within 2 min or so, to the response of a well-developed network structure.

Neutral vs Selective Solvents. Extensive studies of η^* and other behavior in solutions of diblock styrene–bu-

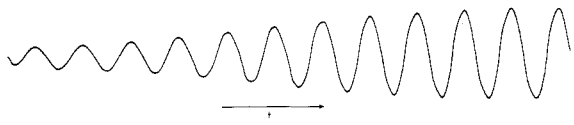

Figure 20. Recovery of topological structure induced by mechanical oscillations. Sample was a cold-loaded solution of polymer 1315, at $c = 0.3272$ (where $c_s \cong 0.32$). Initially liquidlike due to loading degradation, the sample changed rapidly after the onset of testing at $\omega = 0.15\ s^{-1}$ and $\gamma^0 = 0.0075$. The stress amplitude grew and the phase lag (not shown) decreased, as the sample acquired solidlike properties associated with a three-dimensional microstructure.

tadiene copolymers in *selective* solvents have been reported by Watanabe et al.[12,13] Their materials behaved as yield-stress liquids in steady flow but generally as solids in oscillatory testing. Major differences exist between their η^* data and ours, which we believe to be due primarily to intrinsic differences between neutral-solvent systems and selective-solvent systems.

(a) Phase Angle. For $\gamma^0 \leq 0.03$ ($\theta_i \leq 1°$), they found that $\phi = 0$ for all ω—i.e., true solidlike (elastic) behavior. Our systems registered at least $\phi = 20°$, even at much lower amplitude ($\gamma^0 \leq 0.001$).

(b) Structural Stability. They observed no structural degradation in testing at $\gamma^0 = 0.03$; no ϕ-changes resulted from such measurements. Our solutions indicated that structural changes could occur below $\gamma^0 = 0.001$ and that much of the solidlike character (interpreted here as three-dimensional connectivity) was lost when γ^0 exceeded about 0.01.

(c) $\eta'(\gamma^0)$. The maximum in $\eta'(\gamma^0)$ here—Figures 10b, 11, and 12—was not observed in the other work.[12,13]

(d) Nonlinearities. Output stresses became nonsinusoidal for Watanabe et al. only when $\gamma^0 \geq 0.06$, leading to a flat-topped waveform similar to ours in Figure 15a. Most of our data agreed, in that stresses were sinusoidal over the whole γ^0-range examined (to 0.001), but when Δc was small—say, $\Delta c < 0.005$—stresses exhibited severe and unique nonlinearities.

The reasons for all these differences can be traced to the differing physical states of the respective microstructures. In the selective solvent (SS) systems (when the polymer contains hard blocks) the solvent is virtually excluded from one of the phases—e.g., the dispersed cores can be glassy—while, for neutral solvent (NS) systems, the phases are equally solvated. Therefore, structural changes for SS systems (when the polymer contains hard blocks) cannot arise at low γ^0 because polymer chain ends are immobilized in the hard phase. No transfer of molecular blocks between cores can occur, nor partial pullout of blocks from cores. Perhaps most importantly for explaining the ϕ-differences, there is essentially no interface mobility for SS materials, which means that oscillating deformations of the bulk material cannot cause a chain with one end "trapped" in a domain to flow around the core surface to follow the external motion. Thus, like ordinary rubbery solids, SS solutions behave as linear elastic solids at small-to-moderate γ^0 and dissipative phenomena ($\phi > 0$) are not easy to detect.

For NS solutions, on the other hand, all phases are solvated and provide chains with abundant mobility. Because interface mobility is high, chains can be "dragged" around the periphery of a core by an external deformation, giving rise to a flow process with $\phi > 0$ even for intact microstructures. Thermodynamic force barriers to molecular migration between cores, based in a broad interphase,[24] are very weak because of solvent dilution and the resulting small composition gradients in such an interphase. These characteristics of "weakness" are exaggerated when Δc is small, since some of the lower M polymers in the MWD are not yet segregated into microphases and cannot participate in the microstructure.

Thus, NS systems are easily disrupted; the bizarre cyclic nonlinearities seen with small Δc (Figures 14 and 15) were probably due to τ_y being so small that it was exceeded by $\tau(t)$ in the middle of the cycle. However, the corresponding network alteration was apparently due only to partial block pullout from cores, since solidlike behavior reappeared during the cycle. The peaks in Figure 15c, for example, indicate restored solid (elastic) behavior, following a preceding interval of flat shoulder characteristic of a liquidlike yielding. Analysis of this situation[22] will be presented elsewhere.[20]

Acknowledgment. This work was supported by the Polymer Program of the National Science Foundation, through Grant DMR76-83679.

References and Notes

(1) Hansen, P. J.; Hugenberger, G. S.; Williams, M. C. *Proceedings 28th Macromolecular Symposium, IUPAC*; University of Massachusetts: Amherst, July 1982; p 781.
(2) Leary, D. F.; Williams, M. C. *J. Polym. Sci., Polym. Phys. Ed.* **1973**, *11*, 345–358.
(3) Leary, D. F.; Williams, M. C. *J. Polym. Sci., Polym. Phys. Ed.* **1974**, *12*, 265–287.
(4) Henderson, C. P.; Williams, M. C. *J. Polym. Sci., Polym. Phys. Ed.* **1985**, *23*, 1001–1029.
(5) Henderson, C. P.; Williams, M. C. *Polymer* **1986**, *26*, 2026–2038.
(6) Pico, E. R.; Williams, M. C. *J. Polym. Sci., Polym. Phys. Ed.* **1977**, *15*, 1585–1600.
(7) Pico, E. R.; Williams, M. C. *Polym. Eng. Sci.* **1977**, *17*, 573–581.
(8) Pico, E. R.; Williams, M. C. *J. Appl. Polym. Sci.* **1978**, *22*, 445–457.
(9) Hansen, P. J.; Williams, M. C. *Polym. Eng. Sci.* **1987**, *27*, 586–597.
(10) Paul, D. R.; St. Lawrence, J. E.; Troell, J. H. *Polym. Eng. Sci.* **1970**, *10*, 70–78.
(11) Kotaka, T.; White, J. L. *Trans. Soc. Rheol.* **1973**, *17*, 587–616.
(12) Watanabe, H.; Kotaka, T.; Hashimoto, T.; Shibayama, M.; Kawai, H. *J. Rheol.* **1982**, *26*, 153–179.
(13) Watanabe, H.; Kotaka, T. *J. Soc. Rheol. Jpn.* **1980**, *8*, 26.
(14) Osaki, K.; Kim, B.; Kurata, M. *Polym. J.* **1978**, *10*, 353.
(15) Pico, E. R.; Williams, M. C. *Nature (London)* **1976**, *259*, 388–389.
(16) Walters, K. *Rheometry*; Chapman and Hall: London, 1975.
(17) *Instruction Manual for R17 Weissenberg Rheogoniometer*; Sangamo Controls, Ltd.; Sussex, Great Britain.
(18) Onogi, S.; Matsumoto, T.; Warashina, Y. *Trans. Soc. Rheol.* **1973**, *17*, 175–190.
(19) Matsumoto, T.; Hitomi, C.; Onogi, S. *Trans. Soc. Rheol.* **1975**, *19*, 541–555.
(20) Hugenberger, G. S.; Williams, M. C., manuscript in preparation.
(21) Hugenberger, G. S. M.S. Thesis, University of California, Berkeley, 1982.
(22) Hugenberger, G. S., unpublished studies, Chemical Engineering Department, University of California, Berkeley, Dec 1983.
(23) Jones, L. G.; Brodkey, R. S. In *Proceedings of the 5th International Congress on Rheology*; Onogi, S., Ed.; University of Tokyo: Tokyo, 1972; Vol. 2, p 267.
(24) Henderson, C. P.; Williams, M. C. *J. Polym. Sci., Polym. Lett. Ed.* **1979**, *17*, 259–261.